CERN–TH/95–75

Production of heavy quarks and heavy quarkonia

Gerhard A. Schuler

Theory Division, CERN
CH-1211 Geneva 23, Switzerland
E-mail: schulerg@cernvm.cern.ch

Abstract

Uncertainties in the next-to-leading-order calculations of heavy-quark (Q) production are investigated. Predictions for total cross sections, single-inclusive distributions of heavy quarks and heavy flavoured hadrons, as well as for $Q\bar{Q}$ correlations, are compared with charm and bottom data.

The description of heavy-quarkonium production requires a separation of the short-distance scale of $Q\bar{Q}$ production, which is set by the heavy-quark mass from the longer-distance scales associated with the bound-state formation. Various factorization approaches are compared, in particular with respect to the different constraints imposed on the colour and angular-momentum states of the $Q\bar{Q}$ pair(s) within a specific quarkonium state. Theoretical predictions are confronted with data on heavy-quarkonium production at fixed-target experiments and also at $p\bar{p}$ colliders, where fragmentation gives the leading-twist cross section in $1/p_T^2$ and $1/m^2$ at high transverse momentum.

---

[a] Heisenberg Fellow.

CERN–TH/95–75
March 1995

1 Production of heavy quarks

1.1 Theoretical status

Total cross sections and single-inclusive distributions of open heavy-quark production have been calculated in perturbative QCD (pQCD) to next-to-leading-order (NLO) accuracy for essentially all high-energy reactions, hadroproduction [1], photoproduction [2], leptoproduction (deep-inelastic lepton–nucleon scattering) [3], $\gamma\gamma$ collisions [4], and deep-inelastic $e\gamma$ scattering [5]. In the case of photo- and hadroproduction, the NLO calculations have even been implemented in a Monte Carlo programme [6], such that also double-differential distributions can be studied. Attempts are ongoing to develop such an exclusive programme also for deep-inelastic scattering [7].

In pQCD, the differential cross section of heavy-quark (Q) production in the collision of hadrons A and B is given by the factorized expression

$$d\sigma[AB \to Q\bar{Q}X](p_A, p_B) = \sum_{i,j} \int dx_1\, dx_2 f_{i/A}(x_1, \mu_F^2)\, f_{j/B}(x_2, \mu_F^2) d\hat{\sigma}[ij \to Q\bar{Q}X'](x_1 p_A, x_2 p_B, \mu_F, \mu_R)\ . \quad (1)$$

Here i, j represent the interacting partons (gluons, light quarks and antiquarks) and the functions $f_{i/A}(x, \mu_F^2)$ are their number densities, the parton distribution functions (PDF) evaluated at momentum fraction x and factorization scale μ_F. The short-distance cross section $\hat{\sigma}$ is calculable as a perturbation series in $\alpha_s(\mu_R)$ where the strong coupling constant is evaluated at the renormalization scale μ_R. Leading-order (LO) diagrams for heavy-quark hadroproduction are shown in Fig. 1.

The obvious question is, of course, whether pQCD does describe the experimental data on charm and bottom production. To answer this question the uncertainties in the theoretical predictions have to be investigated. These arise from four main sources:

1. The heavy-quark mass m_Q. Conservative ranges are $1.2 < m_c < 1.8\,\mathrm{GeV}$ and $4.5 < m_b < 5.0\,\mathrm{GeV}$.

2. The size of unknown higher-order corrections. An estimate may be obtained by varying the factorization scale μ_F and the renormalization scale μ_R around their 'natural' value $\mu_R = \mu_F = m_Q$, say between $m/2$ and $2m$. In the case of the charm quark, one has to note that most PDF $f_{i/H}(x, \mu_F^2)$ are not valid for $\mu_F \lesssim 2\,\mathrm{GeV}$ and that the running of $\alpha_s(\mu_R^2)$ is no longer purely perturbative for $\mu_R \lesssim m_c/2$. Proper error estimates are therefore not as easy as in the case of the b quark (see below).

3. The value of the QCD scale Λ and the shape of the PDF. Since these are strongly correlated (in particular Λ and the gluon density), the choice of different Λ values (in $60 < \Lambda_5 < 300\,\mathrm{MeV}$, say) in the partonic cross sections should

ideally be accompanied by parametrizations of PDF that have been fitted with those values of Λ. However, LEP data (and also the τ hadronic width) favour Λ values that are almost a factor of two larger than is found in fits to deep-inelastic scattering data. In turn, one does not cover the full range of uncertainty in Λ when restricting to the available PDF parametrizations. In particular, the cross sections may be larger since larger values of Λ imply larger values of α_s. In the absence of fits with Λ frozen to the desired values one may choose [8] to simply change the value of Λ in the partonic cross sections.

4. Non-perturbative effects such as heavy flavoured hadron formation and the intrinsic k_T of the incoming partons.

1.2 Low-energy total cross sections

In the case of charm production it turns out that the biggest uncertainty arises from the variation of m_c. In ref. [8] it is found that predictions of the lowest and largest values of the total charm cross section in hadroproduction may differ by up to a factor of 10 from the central value (i.e. the highest value is a factor of 100 larger than the lowest one)! Predictability substantially improves when increasing the quark mass: for b quarks, the theoretical error is reduced to a factor of ± 2–3. Both for charm and for bottom, the predicted total cross sections are in reasonable agreement with recent data (Fig. 2); the charm data are claimed to be consistent with a charm-quark mass of 1.5 GeV [8].

The uncertainty bands of the theoretical predictions in Fig. 2 represent the *maximum variation* of the cross sections in a parameter range defined as follows [8]. The scale μ_R was varied in $[m_Q/2, 2m_Q]$ and Λ_4 in $[100, 300]$ MeV in order to account for a range of uncertainty in Λ wider than is provided by PDF fits. However, only two particular sets of PDF parametrizations (one for the proton and one for the pion [9]) were chosen with $\Lambda_4 = 190$ MeV. Hence the correlation between Λ and the (nucleon and pion) PDF was not properly taken into account. The mere variation of Λ overestimates the associated uncertainty.

The scale μ_F was also varied in $[m_b/2, 2m_b]$ in the case of bottom, but kept constant at $2m_c$ in the case of charm since the chosen PDF parametrizations [9] are not valid at smaller scales. The choice $\mu_F = 2m_c$ maximizes the values of the PDF for most values of x and in turn of the charm cross sections. Moreover, PDF decrease (eventually non-perturbatively) as $\mu_F^2 \to 0$. Finally, the lowest allowed value of μ_R ($m_c^{min}/2 = 0.6$ GeV), together with the largest value of Λ (300 MeV), gives an α_s value of 1.21, which is certainly beyond QCD perturbation theory. In conclusion, the error bands in ref. [8] are fairly pessimistic, in particular for charm, and values of m_c smaller than 1.5 GeV are favoured by the data.

The question whether the NLO calculation can accommodate the hadroproduction data for $m_c = 1.5$ GeV was also addressed in ref. [10]. The cross section for the choice $\mu_R = \mu_F = m_c = 1.5$ GeV (and the PDF parametrization GRV [11]

that extends down to $\mu_F \sim 0.6\,\mathrm{GeV}$) lies a factor of 2–3 below the data (Fig. 3). A word of caveat on the data shown in Fig. 3 on the total $c\bar{c}$ production cross section from pp and pA interactions is in order.

First, in fixed-target experiments mostly single charmed mesons in the region $x_F > 0$ are measured. Additional, poorly known information is needed to convert $\sigma(D/\bar{D})[x_F > 0]$ into $\sigma[c\bar{c}]$. So far only premature extractions of $\sigma[c\bar{c}]$ exist, obtained by simple assumptions on $\sigma(\Lambda_c)$, $\sigma(D_s)$, the x_F distributions outside the measured range, in particular in pA collisions, the distortion of the x_F distributions due to non-perturbative effects, etc. This explains (at least partly) the spread in the low-energy ($\sqrt{s} \lesssim 40\,\mathrm{GeV}$) data shown in Fig. 3.

Second, the ISR data ($53 < \sqrt{s} < 62\,\mathrm{GeV}$), inferred from lepton measurements in coincidence with a reconstructed charmed hadron, are presumably too large due to the assumed shape of the production cross sections: flat distributions in x_F for the Λ_c and $(1 - x_F)^3$ for the D. Restricting to the most recent experiments only consistency is found [8, 10] between the data (Figs. 2 and 3) and these data agree rather well with $\mu_R = \mu_F = m_c = 1.3\,\mathrm{GeV}$ in the NLO calculation using the GRV PDF [11]. The result is similar (Fig. 3) with the MRS distributions [12] and $\mu_R = \mu_F = 2m_c$ where now the large μ_R requires an even smaller charm-quark mass, $m_c \sim 1.2\,\mathrm{GeV}$. Note that such small values of m_c suggest that the bulk of the total cross section comes from invariant masses smaller than $2m_D$.

The theoretical uncertainty is smaller in photoproduction: there the Born cross section starts at $O(\alpha_s)$, compared to $O(\alpha_s^2)$ in hadroproduction, and also only a single parton density enters. For example, the charm cross section can now be calculated up to a factor of about 3 [8]. The theoretically better-controlled b-quark cross section has unfortunately not yet been measured in photoproduction; the forthcoming measurement in γp collisions at HERA is eagerly awaited.

Additional tests of heavy-quark production will soon also be possible in electroproduction of heavy quarks at HERA and in electron–photon collisions at LEP2. The most reliable predictions can be made for heavy-quark production in $\gamma\gamma$ collisions. Even for c quarks, the total uncertainty is only about $\pm(30$–$35)\%$ [4]. The experimental situation is so far controversial: taken at face value, the cross section seems to fall when going from Tristan [13] ($\sqrt{s}_{ee} \sim 60\,\mathrm{GeV}$) to LEP1 [14] ($\sqrt{s}_{ee} \sim 90\,\mathrm{GeV}$)!

1.3 Single-inclusive distributions

Single-inclusive distributions can be calculated in pQCD by folding the (NLO) cross sections of heavy-quark production with the corresponding (NLO) fragmenting function, e.g. $c \to D + X$. In general, the x_F and p_T spectra of the heavy-flavour hadron will be softer than those of the mother heavy-quark. In the case of charm hadroproduction, the measured D-meson p_T distribution is considerably harder than the one calculated in NLO perturbation theory. Since the

c.m.s. energies are small ($\sqrt{s} = 20$–$40\,\mathrm{GeV}$), it appears unlikely that the discrepancy can solely be resolved by yet higher-order corrections. Rather the description of differential charm distributions requires the inclusion of non-perturbative effects. These may arise from the intrinsic transverse momenta k_T of the incident partons and/or higher-twist corrections in the hadronization.

The effect of intrinsic k_T is well established in the Drell–Yan process and its inclusion gives also reasonable agreement [8] for D-meson p_T distributions. In fact, photoproduction data are reproduced with k_T values as they are also observed in the Drell–Yan process, i.e. $\langle k_T^2 \rangle^{1/2} \sim 0.7\,\mathrm{GeV}$. On the other hand, hadroproduction data require values that are as large ($\langle k_T^2 \rangle^{1/2} \sim 1.4\,\mathrm{GeV}$) as the charm-quark mass. Further studies are certainly needed, in particular on the strong correlation of k_T with m_c (larger m_c yields harder p_T spectra and, in turn, allows smaller k_T values).

Distributions in x_F have so far only be measured for charmed hadrons and do not at all agree with the pQCD predictions (they are too soft), even after inclusion of the k_T effects [8]. Indeed, an agreement must not be expected in the first place, as factorization, underlying the perturbative approach, is valid only at large p_T and hence breaks down at large x_F. Additional non-perturbative contributions associated with the hadronization become important: The enhanced production of D-mesons whose light valence quark is of the same flavour as one of the valence quarks in the beam hadron (leading-particle effect) and the dragging of charm quarks in the colour field of the beam fragments (colour-drag effect). Indeed, a fragmentation model that contains these effects, such as the Lund string fragmentation one, successfully describes the observed spectra. An alternative explanation [15] invokes new production mechanisms for hard processes at large x_F through terms that are formally higher-twist effects $\propto 1/m_Q^2$ but are enhanced by inverse powers of $1 - x_F$.

1.4 $Q\bar{Q}$ correlations

In leading order, pQCD predicts that the heavy quark and heavy antiquark are produced exactly back-to-back (Fig. 1), implying $p_T(Q\bar{Q}) = 0$ and $\Delta\phi = \pi$, where $p_T(Q\bar{Q})$ is the transverse momentum of the pair and $\Delta\phi$ the angle between the projections of the momenta of the pair onto the transverse (w.r.t. beam axis) plane. NLO corrections, as well as non-perturbative effects, can cause a broadening of these distributions. The question whether NLO predictions can account for the available experimental data in hadro- and photoproduction of charmed particles was addressed in ref. [8]. Agreement with data was found for the $\Delta\phi$ distribution after inclusion of a modest intrinsic transverse momentum $\langle k_T^2 \rangle^{1/2} \sim 0.7$–$1\,\mathrm{GeV}$.

The theoretical $p_T(Q\bar{Q})$ distributions, on the other hand, are too soft unless much larger k_T values are used. Although it is mostly the intrinsic k_T of gluons that enters heavy-quark production and not the k_T of quarks that is known from

the Drell–Yan process to be of the order of 700 MeV, it yet appears unreasonable to have a k_T that is of the order of the hard scale, namely $k_T \sim m_Q$. Three possible explanations come up. First higher-order corrections can broaden the $p_T(Q\bar{Q})$ shape. After all, the $O(\alpha_s^3)$ calculation, although being of NLO accuracy for the total cross section and single-inclusive distributions, is still of leading order for the $\Delta\phi$ and $p_T(Q\bar{Q})$ ones. Second, further non-perturbative contributions besides k_T could be significant. And third, experimental high-$p_T(c\bar{c})$ data are still rather limited in statistics and might possibly come down. New measurements of charm hadroproduction by WA92 are on their way . The different hypotheses to explain the high-$p_T(Q\bar{Q})$ discrepancy can also be tested in photoproduction at HERA where high-$p_T(Q\bar{Q})$ data should soon become available.

1.5 Bottom production at collider energies

Owing to its heavier mass, not only the total b cross section but also differential distributions of the b-quark and b-flavoured hadrons can be predicted with higher accuracy (at least, if $m_Q/\sqrt{s}$ is not too small). In fact, the p_T distribution measured at both 630 GeV and 1.8 TeV is now found to be consistent (Fig. 4) with the NLO predictions [8]: On the one hand, the experimental data from the Tevatron 'came down' through improved b tagging, $b \to J/\psi$, ψ' via secondary b vertices, $B \to J/\psi + K^{(*)}$, $b\bar{b}$ correlations, $b \to \mu X$ identification in D0. On the other hand, the theoretical prediction 'came up', partly because PDF are now known to steeply increase in the relevant x range [16].

The biggest change in ref. [8] compared to previous estimates is, however, that Λ is allowed to be as large as the central LEP value ($\Lambda_5 \sim 300$ MeV or $\Lambda_4 \sim 420$ MeV). The upper curve in Fig. 4 is obtained by stretching all parameters to their extremes: small quark mass ($m_b = 4.5$ GeV), small renormalization scale ($\mu_R = \mu_F = \sqrt{p_T^2 + m_b^2}/2$), and large QCD scale ($\Lambda_5 = 300$ MeV). Yet, at the same time the MRSA PDF parametrization [17] with $\Lambda_5 = 151$ MeV is being used. First estimates [8] indicate that varying Λ within a limited range, without refitting the PDF, is not as large an overestimate of the systematic effect of the Λ uncertainty on the b cross section as one might expect at first. Given the potential sensitivity of the b cross section on small-x effects, further theoretical studies should certainly be pursued.

2 Bound-state production

The production of quarkonium states below the open charm/bottom thresholds presents a particular challenge to QCD. Because of the relatively large quark masses, c and b production are perturbatively calculable, see previous section. However, the subsequent transition from the predominantly colour-octet $Q\bar{Q}$ pairs to physical quarkonium states introduces non-perturbative aspects. Three models

of bound-state formation are discussed in the literature. In order of increasing sophistication, these are the colour-evaporation model [18, 19], the colour-singlet model [20, 19], and the one based on a new factorization formula.

In QCD, the total angular momentum J, the parity P, and the charge conjugation C are exactly conserved quantum numbers. Hence the energy eigenstates $|H\rangle$ of heavy quarkonium can be labelled by the quantum numbers J^{PC} (besides a quantum number $n = 1, 2, \ldots$, to distinguish states identical apart from their mass M as the 1^{--} states J/ψ and ψ'). Phenomenologically very successful is the non-relativistic potential model, in which $|H\rangle$ is assumed to be a pure quark–antiquark state $|Q\bar{Q}\rangle$. Obviously, the $Q\bar{Q}$ pair must then be in a colour-singlet state $\underline{1}$ and in an angular-momentum state $^{2S+1}L_J$ that is consistent with the quantum numbers J^{PC} of the meson ($P = (-1)^{L+1}$, $C = (-1)^{L+S}$)

$$\text{potential model}: \quad |H(nJ^{PC})\rangle = |Q\bar{Q}(n^{2S+1}L_J, \underline{1})\rangle \ . \tag{2}$$

Here $S = 0, 1$ is the total spin of the quark and antiquark, $L = 0, 1, 2, \ldots$ or $S, P, D, \ldots$ is the orbital angular momentum, J is the total angular momentum, and n denotes the principal quantum number.

2.1 Colour-singlet model

In the colour-singlet model, the dominant production mechanism of a heavy quarkonium is assumed to be the one in which the quarkonium is produced *at short distances* in a colour-singlet $Q\bar{Q}$ state with the correct quantum numbers. Hence the cross section is given by the factorized form ($v = x_F$, p_T, ...):

$$\frac{d\sigma[H(nJ^{PC})](s,v)}{dv} = F_{nL}\,\frac{d\sigma[Q\bar{Q}(n^{2S+1}L_J, \underline{1})](s,v)}{dv} \ . \tag{3}$$

The non-perturbative probability F_{nL} for the $Q\bar{Q}$ pair to form the bound state H is given in a calculable way in terms of the radial wave function or its derivatives

$$F_{nL} \propto \frac{|R^{(L)}_{nL}(0)|^2}{M_H^{3+2L}} \tag{4}$$

and can either be calculated using a phenomenological potential or extracted from the H decay widths that are given by an expression similar to (3) [19].

Actually, (3) gives the dominant cross section only if the relevant momentum scale Q is of the order of the heavy quark mass. An example is the total hadroproduction cross section of J/ψ where $Q^2 \sim \hat{s} \sim 4m^2$. At large scale Q, however, the short-distance production becomes suppressed by a factor m^2/Q^2 with respect to production via fragmentation that then gives the leading-twist cross section in $1/Q^2$ and $1/m^2$. A long-known example [21] is J/ψ production in Z^0 decays where $c\bar{c}$ pair production followed by the fragmentation $c \to J/\psi$ dominates over $Z^0 \to J/\psi gg$.

Similarly, fragmentation processes start to dominate $p\bar{p} \to H + X$ at high p_T [22]. In this case, important contributions arise from gluon fragmentation

$$\frac{d\sigma[p\bar{p} \to H(p) + X](s, p_T)}{dp_T} = \int_0^1 dz \; \frac{d\hat{\sigma}[p\bar{p} \to g(p_T/z) + X](s, p_T, \mu)}{dp_T} \; D_{g\to H}(z, \mu, m) \; . \tag{5}$$

The fragmentation functions $D_{a\to H}(z, \mu, m)$ specify the probability for partons a (gluons, light and heavy quarks) to hadronize into the hadron H as a function of its longitudinal momentum fraction z relative to a. Large logarithms of p_T/μ in the parton cross sections $\hat{\sigma}$ are avoided by choosing the (arbitrary) factorization scale μ of the order of the large scale p_T. Large logarithms of μ/m then necessarily appear in the fragmentation functions $D_{a\to H}(z, \mu, m)$, but they can be summed up by evolving the "input" distributions $D^{(0)}_{a\to H}(z) \equiv D_{a\to H}(z, m, m)$ with the standard evolution equations.

In the colour-singlet model, the fragmentation functions at the input scale m, $D^{(0)}_{a\to H}(z)$ can be calculated as a series in $\alpha_s(m)$ by assuming that they take the same factorized form as (3). For example, the lowest-order diagrams that contribute to gluon fragmentation into J/ψ are $g \to c\bar{c}(^3S_1, \underline{1})gg$, so that

$$D^{(0)}_{g\to J/\psi}(z) = \left(\frac{\alpha_s(m)}{m}\right)^3 |R_{1S}(0)|^2 f(z) + O(\alpha_s^4) \; , \tag{6}$$

where $f(z)$ is a calculable function. Note that the kinematic regime in which the $a \to H$ fragmentation graphs become important occurs when the lab-frame energy E_a of the parton a is large, but its squared four-momentum p_a^2 is close to the square of the charmonium bound-state's mass $\approx 4m^2$. Terms subdominant in the ratio p_a^2/E_a^2 are therefore neglected.

In contrast to S-wave fragmentation functions [22, 23], the colour-singlet contributions to fragmentation functions into χ_{QJ} state are, however, singular. The process $g \to c\bar{c}(^3P_J, \underline{1}) + g$ diverges logarithmically [24] (analogously $c \to c\bar{c}(^3P_J, \underline{1}) + c$ [25])

$$D^{(0)}_{g\to\chi_J}(z) = \frac{\alpha_s^2(m)}{9\pi} \; \frac{|R'_P(0)|^2}{m^5} \left\{ (2J+1) \left[\frac{z}{(1-z)_+} + \ln\frac{m}{\epsilon_0} \, \delta(1-z) \right] + r_J(z) \right\} \; . \tag{7}$$

Here the infrared divergence, associated with the soft limit of the final-state gluon has been made explicit by the introduction of a lower cutoff ϵ_0 on the gluon energy in the quarkonium rest frame. The presence of the infrared sensitive term clearly spoils the factorization assumption of the colour-singlet model.

In order to still separate the long- and short-distance contributions (at least) a second non-perturbative parameter has to be introduced

$$D^{(0)}_{g\to\chi_J}(z) = \frac{d_1^{(J)}(z; \lambda)}{m^2} \, O_1 + d_8(z) \; O_8(\lambda) \; . \tag{8}$$

The first term in (8) describes the emission of a perturbative gluon with energy above some cutoff λ

$$\begin{aligned} O_1 &= \frac{9}{2\pi}\,|R'_P(0)|^2 \\ d_1^{(J)}(z,\lambda) &= \frac{2}{81}\frac{\alpha_s^2(m)}{m^3}\left\{(2J+1)\left[\frac{z}{(1-z)_+}+\ln\frac{m}{\lambda}\,\delta(1-z)\right]+r_J(z)\right\}\ . \end{aligned} \tag{9}$$

In the second term

$$\begin{aligned} O_8(\lambda) &= \frac{16}{27\pi}\,\alpha_s\ln\frac{\lambda}{\epsilon_0}\,\frac{(2J+1)\,H_1}{m^2} \\ d_8(z) &= \frac{\pi}{24}\,\frac{\alpha_s(m)}{m^3}\,\delta(1-z)\ , \end{aligned} \tag{10}$$

the presence of the infrared scale ϵ_0 indicates that O_8 actually has to be considered as an additional non-perturbative parameter besides $R'_P(0)$, as expression (10) for O_8 can at best give the perturbative part of O_8.

Even with improved P-wave factorization, the colour-singlet model still fails in the description of data on high-p_T prompt charmonium production. Such data now become available at the Tevatron where vertex detectors can be used to separate the charmonium states coming from b quarks from those that are produced by QCD interactions. Through the inclusion of fragmentation mechanisms the theoretical predictions for prompt J/ψ production can be brought to within a factor of 3 of the data [26, 27], close enough that the remaining discrepancy might be attributed to theoretical uncertainties (Fig. 5).

However, this conclusion of a successful description of J/ψ production relies on the postulation of a very large $g \to \chi_{cJ}(1P)$ fragmentation contribution[1] where the χ_{cJ} subsequently decay into $\gamma J/\psi$. Since such a contribution is absent for ψ' the prediction of its production rate falls a factor of 30 below the data (Fig. 5), casting doubts[2] on whether the J/ψ production is correct at all. These doubts are strengthened by the observation that the ratio of ψ' to J/ψ measured at high transverse momenta at the Tevatron is quite compatible [29, 30] with the p_T-integrated fixed-target and ISR data where direct J/ψ production is known [19] to dominate the indirect production via χ_{cJ} decays. Hence the major part of prompt high-p_T J/ψ's should be directly produced rather than originate from radiative χ_{cJ} decays.

The breakdown of the simple factorization into a single long-distance matrix element and a short-distance Wilson coefficient, discussed above for gluon fragmentation into P-wave quarkonia, has, in fact, previously been pointed at for

[1] This large contribution follows from an optimistic choice of O_8 in (8).

[2] The ad hoc introduction of (not-yet) observed charmonium states above the $D\bar{D}$ threshold such as higher P-wave or D-wave states appears quite questionable. Only with very optimistic production rates and branching fractions into ψ' can one account for the observed rate for prompt ψ' production [28].

the cases of B-meson decays into χ_{cJ} [31], hadronic χ_{QJ} decays, and total cross sections of χ_{QJ} hadroproduction [19]. Also these analyses showed that, even if the colour-singlet model is extended through the inclusion of colour-octet mechanisms for P-wave states (analogues of the O_8 term in (8), see also section 2.3), the model cannot accommodate for all the data on quarkonium production and decays.

It must therefore be concluded that also in the case of S-waves, a generalization of the naïve factorization à la (3,6) is necessary, at least in cases where the colour-singlet mechanism is suppressed by a short-distance coefficient, i.e. by a high power of $\alpha_s(m)$, cf. (6). A factorization of long- and short-distance physics more generalized than the one assumed in the colour-singlet model will be presented in section 2.3. First, however, a quarkonium production-model diametrally opposite to the colour-singlet model is discussed.

2.2 Colour-evaporation model

The starting, i.e. perturbatively calculated cross section for heavy quarkonium production in the colour-evaporation model is the (usual) cross section of open heavy-quark pair production that is summed over all spin and colour states. Hence all the information on the non-perturbative transition of the $Q\bar{Q}$ pair to the heavy quarkonium H of quantum numbers J^{PC} is contained in "fudge factors" $F_{nJ^{PC}}$ that a priori may depend on all quantum numbers

$$\frac{d\sigma[H(nJ^{PC})](s,v)}{dv} = F_{nJ^{PC}}\,\frac{d\tilde{\sigma}[Q\bar{Q}](s,v)}{dv}\ . \tag{11}$$

In (11) $\tilde{\sigma}[Q\bar{Q}]$ is the total "hidden" cross section of (open) heavy-quark production calculated by integrating over the $c\bar{c}$ pair mass (in the case of charmonium) from $2m_c$ to $2m_D$. For example, in hadronic collisions at high energy, the dominant production mechanism is gluon fusion, so that (cf. (1)):

$$\begin{aligned}\tilde{\sigma}[c\bar{c}](s) = \int_{4m_c^2}^{4m_D^2} d\hat{s} \int dx_1 dx_2 \\ f_{g/A}(x_1,m^2) f_{g/B}(x_2,m^2) \widehat{\sigma}[gg\to c\bar{c}X](\hat{s})\delta(\hat{s}-x_1x_2s)\ .\end{aligned} \tag{12}$$

Note that $\tilde{\sigma}[c\bar{c}]$ is the spin-summed cross section and that the heavy-quark pair can be both in a colour-singlet and a colour-octet state (in LO, $q\bar{q}$ annihilation produces only colour-octet $c\bar{c}$ pairs, while gg fusion also leads to colour-singlet states). The colour-octet cross section is the dominant one. The $c\bar{c}$ configuration arranges itself into a definite outgoing charmonium state by interacting with the collision-induced colour field ("colour evaporation"). During this process, the c and the $\bar{c}$ either combine with light quarks to produce charmed mesons, or they bind with each other to form a charmonium state.

As shown in ref. [30] more than half of the subthreshold cross section $\tilde{\sigma}[c\bar{c}]$ in fact goes into open charm production (assuming $m_c < m[\eta_c]/2 \sim 1.5\,\mathrm{GeV}$); the additional energy needed to produce charmed hadrons is obtained (in general non-perturbatively) from the colour field in the interaction region. The yield of all charmonium states below the $D\bar{D}$ threshold is thus only a part of the total sub-threshold cross section: in this aspect the modern version of the model [30] is a generalization of the original colour-evaporation model [18, 19], which neglected the contribution of $\tilde{\sigma}[c\bar{c}]$ to open charm production. Using duality arguments, it equated $\tilde{\sigma}[c\bar{c}]$ to the sum over the charmonium states below the $D\bar{D}$ threshold.

Neither the division of $\tilde{\sigma}[c\bar{c}]$ into open charm and charmonia nor the relative charmonium production rates are specified by the generalized colour-evaporation model. Hence its essential prediction is that the dynamics of charmonium production is that of $\tilde{\sigma}[c\bar{c}]$, i.e. the energy dependence, x_F- and p_T-distributions of H are identical to those of the free $c\bar{c}$ pair. In particular, ratios of different charmonium production cross sections should be energy-, x_F-, and p_T-independent. In other words, the non-perturbative factors $F_{n^{J^{PC}}}$ should be universal constants whose values may, however, depend on the heavy-quark mass. In contrast to earlier expectations [19], a recent comprehensive comparison of the generalized colour-evaporation model with data indeed confirmed these expectations [30].

Figure 6 shows the ratio of J/ψ production from the decay $\chi_c \to \gamma\ J/\psi$ to the total J/ψ production rate, which provides a measure of the $\chi_c/(J/\psi)$ rate, and Fig. 7 shows the measured $\psi'/(J/\psi)$ ratio. Both ratios are found to be independent of the incident energy, the projectile (pion or proton), and the target (from protons to the heaviest nuclei). Moreover, it is noteworthy [29, 30] that the ratio $\psi'/(J/\psi)$ measured at high transverse momenta at the Tevatron is quite compatible with the p_T-integrated fixed-target and ISR data (Fig. 8). Also the available bottomonium data agree with constant production ratios [30].

Figures 9 and 10 show the energy dependence of J/ψ and Υ production in hadronic collisions; the agreement with data over a wide range is rather impressive. Because the data generally give the sum of Υ, Υ' and Υ'' production, the measured cross section for the sum of the three Υ states in the dilepton decay channel is shown, denoted by $B(d\sigma/dy)_{y=0}$. Using the average values of the Υ'' to Υ and Υ' to Υ production ratios, 0.53 ± 0.13 and 0.17 ± 0.06, respectively, fits [30] to the data in Figs. 9 and 10 yield

$$F_{11^{--}} \approx \begin{cases} 2.5 \times 10^{-2} & \text{charm} \\ 4.6 \times 10^{-2} & \text{bottom} \end{cases} . \tag{13}$$

The hidden heavy-flavour cross sections $\tilde{\sigma}[Q\bar{Q}]$ in Figs. 9 and 10 were calculated in NLO using the MRS D$-'$ parametrization [12] of PDF with $\mu_F = \mu_R = 2m_c = 2.4\,\mathrm{GeV}$ and $\mu_F = \mu_R = m_b = 4.75\,\mathrm{GeV}$, respectively. These parameters provide an adequate description of open heavy-flavour production [10], cf. section 1. Results similar to (13) are obtained if one uses other choices of the

parameters that are tuned to the open heavy-flavour data, for instance the GRV parametrization [11] with $\mu_F = \mu_R = m_Q$, $m_c = 1.3\,\mathrm{GeV}$, and $m_b = 4.75\,\mathrm{GeV}$. From (13) one concludes that the fraction of $\tilde{\sigma}[c\bar{c}]$ producing charmonium rather than open charm is about 10%.

Equally good agreement is found for the energy dependence of J/ψ production with pion beams. However, the fraction of J/ψ in the hidden charm cross section must be slightly higher to reproduce the pion data well, with $F_{11^{--}} = 0.034$ for a good fit. This may well be due to greater uncertainties in the pionic parton distribution functions. Consistency with the colour-evaporation model is also found for the longitudinal momentum dependence of charmonium production. The calculations for the x_F dependence of J/ψ production agree with data (Fig. 11) from low-energy $\bar{p}p$ interactions (where $q\bar{q}$ annihilation is important) up to pp interactions at the highest available energy and out to the largest x_F values probed (where the "intrinsic charm" mechanism could have been important).

Concerning the p_T distribution, the model provides essentially no prediction for low-p_T charmonium production. There is the intrinsic transverse momentum of the initial partons, the intrinsic momentum fluctuations of the colour field which neutralizes the colour of the $c\bar{c}$ system in the evaporation process and, at larger p_T, higher-order perturbative terms. Since there is no way to separate these different contributions in the low-p_T region, the model has no predictive power.

On the other hand, the high-p_T tail should be successfully describable in the colour-evaporation model, presumably with the same normalization (13). The time scale to form a quarkonium bound state is much larger than the one to produce the (compact) $c\bar{c}$ pair. Hence the fraction of the $c\bar{c}$ cross section (in $2m_c < M_{c\bar{c}} < 2m_D$) that becomes a J/ψ (or ψ') should be independent of the $c\bar{c}$ production, i.e. the same for low-p_T and high-p_T processes. By the same argument, the universal ratio of ψ' to J/ψ production, observed experimentally, can depend only on the relative magnitude of the respective wave functions at the origin

$$\begin{aligned} \frac{\Gamma(\psi' \to e^+e^-)}{\Gamma(J/\psi \to e^+e^-)} \left(\frac{M_{J/\psi}}{M_{\psi'}}\right)^3 &= \frac{\sigma(\psi')}{\sigma_{dir}(J/\psi)} \\ &= \left[\frac{1}{1-\sigma(\chi_c \to J/\psi)/\sigma(J/\psi)}\right] \left[\frac{\sigma(\psi')}{\sigma(J/\psi)}\right]_{\mathrm{exp}} . \end{aligned} \tag{14}$$

Relation (14) holds to very good approximation [29, 30]. Note, finally, that gluon fragmentation $gg \to g^\star g$ with $g^\star \to c\bar{c} \to J/\psi$ is part of the lowest-order ($O(\alpha_s^3)$) diagrams describing high-p_T charmonium production in hadronic collisions, while charm fragmentation $gg \to c^\star\bar{c}$ with $c^\star \to J/\psi$ first occurs at $O(\alpha_s^4)$.

2.3 A new factorization approach

The two previous sections discussed two extreme scenarios to describe production cross sections (and decay rates) of heavy quarkonia. In the colour-evaporation model (11), no constraints are imposed on the colour and angular momentum states of the $Q\bar{Q}$ pair. Non-perturbative QCD effects, mediating the transition to the colour-singlet bound state $H(J^{PC})$ containing the $Q\bar{Q}$ pair are assumed to be first universal and secondly negligible for the dynamics of H ($\sqrt{s}$, p_T, etc. dependence). The normalization factors for the various states are not predictable, but once fixed phenomenologically, the model is (surprisingly) successful.

The factorization assumption (3) of the colour-singlet model, on the other hand, says that all non-perturbative effects are contained in a single term that can be expressed as the non-relativistic wave function of the bound state. In turn, relative production rates of different quarkonium states can be predicted. Moreover, different states may have different dynamical dependences since only specific short-distance cross sections contribute to each state. However, the colour-singlet model fails in two respects. First, predictions for S-wave states often are way off, and second logarithmic infrared divergences spoil the factorization in the case of P-waves, cf. section 2.1.

This failure of the colour-singlet model can be traced back to that of the underlying quark potential model. Relativistic corrections are essential for a description that is both consistent for P-wave states and successful for S-wave states. Recently, a rigorous QCD analysis of the annihilation decays of heavy quarkonium has been presented based on recasting the analysis in terms of HQ$\bar{\text{Q}}$ET, an effective field theory designed precisely for this purpose [32]. It allows the separation of long and short distances, where the short-distance contribution may be evaluated perturbatively, i.e. as series in $\alpha_s(m)$. The long-distance part is parametrized in terms of matrix elements, which are organized into a hierarchy according to their scaling with $1/m$.

A similar analysis has been performed in the context of non-relativistic quantum chromodynamics (NRQCD) [33]. In this approach, the calculations are organized in powers of v, the average velocity of the heavy (anti-)quark in the meson rest frame. Contributions of different orders in v are separated according to the "velocity-scaling" rules. This factorization formalism has been extended to the production cross section of heavy quarkonium in processes involving momentum transfers of order m or larger.

The inclusive production cross section of a quarkonium state H and the parton fragmentation function into H take the form:

$$\begin{aligned} \sigma(H) &= \sum_{c=1,8} \sum_{d=6,8,\ldots} \sum_{X} \frac{F_c^{(d)}(X;\lambda)}{m^{d-4}} \langle 0|\mathcal{O}_c^H(d,X;\lambda)|0\rangle \\ D_{a\to H}^{(0)}(z) &= \sum_{c=1,8} \sum_{d=6,8,\ldots} \sum_{X} \frac{d_c^{(d)}(X;z,\lambda)}{m^{d-6}} \langle 0|\mathcal{O}_c^H(d,X;\lambda)|0\rangle \ . \end{aligned} \tag{15}$$

Equation (15) expresses the cross section (and analogously the fragmentation function) as a sum of terms, each of which factors into a short-distance coefficient $F_n(\lambda)$ and a long-distance matrix element $\langle 0|\mathcal{O}_n^H(\lambda)\rangle$ (where $n = \{c, d, X\}$). The coefficients F_n are proportional to the rates for the production of on-shell heavy quarks and antiquarks from initial-state gluons and light quarks, and they can be computed as perturbation series in $\alpha_s(m)$. They depend on all the kinematical variables of the production process. The matrix elements $\langle 0|\mathcal{O}_n^H|0\rangle$ give the probability for the formation of the quarkonium state H from the $Q\bar{Q}$ pair of state n, and can be evaluated non-perturbatively using, for example, QCD sum rules or lattice simulations. The dependence on the arbitrary factorization scale λ in (15) cancels between the coefficients and the operators.

The expansion (15) is organized into an expansion in powers of v^2. Only a finite number of operators contribute to any given order in v^2. Since the coefficients F_n are calculated as perturbation series in $\alpha_s(m)$, eq. (15) is really a double expansion in $\alpha_s(m)$ and v^2. For heavy quarkonia, the two expansion parameters are not independent: $v \approx \alpha_s(mv) > \alpha_s(m)$. Hence corrections of order v^n must not be neglected compared to those of order $\alpha_s^n(m)$. Which terms in (15) actually contribute to the production of a quarkonium $|H\rangle$ depends on both the $\alpha_s(m)$ expansion of F_n and the v^2 expansion of the matrix elements. The latter is determined by the variables that specify a given operator $\mathcal{O}_c^H(d, X)$. These are the dimension d of the operator, and two further variables c and X, which specify the quantum numbers of the heavy $Q\bar{Q}$ pair in the Fock-state expansion of the heavy quarkonium H.

The state of the $Q\bar{Q}$ pair in a general Fock state can be labelled by the colour state of the pair, singlet ($c = 1$) or octet ($c = 8$), and the angular momentum state ${}^{2S+1}L_J$ of the pair denoted by X. The leading term of the Fock-state expansion is the pure $Q\bar{Q}$ state (2) of the potential model. Higher Fock states are suppressed by powers of v, which follow from the velocity-scaling rules [33]. For example, if the $Q\bar{Q}$ in the dominant Fock state $|Q\bar{Q}\rangle$ has angular-momentum quantum numbers ${}^{2S+1}L_J$, then the Fock state $|Q\bar{Q}g\rangle$ has an amplitude of order v only if the $Q\bar{Q}$ pair has total spin S and orbital angular momentum $L + 1$ or $L - 1$ (E1 transition). Necessarily, the $Q\bar{Q}$ pair must be in a colour-octet state. The general Fock-state expansion therefore starts as

$$\begin{aligned} |H(nJ^{PC})\rangle \;=\; & O(1)\,|Q\bar{Q}({}^{2S+1}L_J, \underline{1})\rangle \\ & + O(v)\;\; |Q\bar{Q}({}^{2S+1}(L \pm 1)_{J'}, \underline{8})\; g\rangle \\ & + O(v^2)\; |Q\bar{Q}({}^{2S+1}L_J, \underline{8})\; gg\rangle + \ldots \\ & + \;\ldots\; . \end{aligned} \tag{16}$$

In the case of J/ψ production, for example, one finds up to and including the

order v^2 [33]:

$$\begin{aligned}\sigma(J/\psi) &= \frac{F_1^{(6)}({}^3S_1;\lambda)}{m^2}\langle 0|\mathcal{O}_1^{J/\psi}(6,{}^3S_1;\lambda)|0\rangle \\ &\quad + \frac{F_1^{(8)}({}^3S_1;\lambda)}{m^4}\langle 0|\mathcal{O}_1^{J/\psi}(8,{}^3S_1;\lambda)|0\rangle + O(v^4)\ . \end{aligned} \tag{17}$$

Upon dropping the $O(v^2)$ contribution and identifying $\langle 0|\mathcal{O}_1^{J/\psi}(6,{}^3S_1;\lambda)|0\rangle = 3N_C|R_{1S}(0)|^2/(2\pi)$, eq. (17) reduces to the familiar factorization formula (3) of the colour-singlet model. Generally, the standard factorization formulas of the colour-singlet model, which contain a single non-perturbative parameter, are recovered in the case of S-waves at leading order in v^2.

However, the factorization formula is the sum of two terms in the case of P-waves. In addition to the conventional term, which takes into account the production (or annihilation) of the $Q\bar{Q}$ pair from a colour-singlet P-wave state, there is a second term that involves production (annihilation) from a colour-octet S-wave state. For example, the gluon fragmentation function into χ_{cJ} states ($J = 0, 1, 2$) is [24], cf. (7,8):

$$\begin{aligned}D_{g\to\chi_{cJ}}^{(0)}(z) &= \frac{d_1^{(8)}(z;{}^3P_J;\lambda)}{m^2}\langle 0|\mathcal{O}_1^{\chi_{cJ}}(8,{}^3P_J;\lambda)|0\rangle \\ &\quad + d_8^{(6)}(z;{}^3S_1;\lambda)\langle 0|\mathcal{O}_8^{\chi_{cJ}}(6,{}^3S_1;\lambda)|0\rangle + O(v^2)\ . \end{aligned} \tag{18}$$

The J^{++} state $|\chi_{cJ}\rangle$ consists predominantly of the Fock state $|Q\bar{Q}\rangle$, with the $Q\bar{Q}$ pair in a colour-singlet ${}^3P_J$ state. It also has an amplitude of order v for the Fock state $|Q\bar{Q}g\rangle$, with the $Q\bar{Q}$ pair in a colour-octet ${}^3S_1$, ${}^3D_1$, ${}^3D_2$, or ${}^3D_3$ state:

$$|\chi_{QJ}\rangle = O(1)|Q\bar{Q}({}^3P_J,\underline{1})\rangle + O(v)|Q\bar{Q}({}^3S_1,\underline{8})g\rangle + O(v)|Q\bar{Q}({}^3D_{J'},\underline{8})g\rangle + O(v^2)\ . \tag{19}$$

The Fock state $|Q\bar{Q}\rangle$ contributes to the production at leading order in v^2 through the dimension-8 operator $\mathcal{O}_1^{\chi_{cJ}}(8,{}^3P_J)$. The Fock state $|Q\bar{Q}g\rangle$, with the $Q\bar{Q}$ pair in a colour-octet ${}^3S_1$ state also contributes to the production at the same order in v^2, through the dimension-6 operator $\mathcal{O}_8^{\chi_{cJ}}(6,{}^3S_1)$, because the latter scales as v^{-2} relative to $\mathcal{O}_1^{\chi_{cJ}}(8,{}^3P_J)$.

Equation (18), together with the evolution equations for the matrix elements contain the solution to the problem of the infrared divergence encountered in (7). At leading order in $\alpha_s(m)$, the coefficient $d_1^{(8)}(z;{}^3P_J;\lambda)$ in (18) ($\equiv d_1^{(J)}(z,\lambda)$ in (8,9)) depends logarithmically on the factorization scale λ, while $d_8^{(6)}(z;{}^3S_1;\lambda) \equiv d_8(z)$ in (8,10) is independent of λ. In these coefficients, λ plays the role of an infrared cutoff. The λ-dependence of the short-distance coefficients cancels the λ-dependence of the long-distance matrix elements, for which λ plays the role of an ultraviolet cutoff.

At leading order in v^2 and $\alpha_s(m)$, the dimension-8 matrix element $O_1(\lambda) \equiv \langle 0|\mathcal{O}_1^{\chi_J}(8,{}^3P_J;\lambda)|0\rangle$ is renormalization-scale-invariant, while the dimension-8 matrix element $O_8(\lambda) \equiv \langle 0|\mathcal{O}_8^{\chi_J}(6,{}^3S_1;\lambda)|0\rangle$ has a non-trivial scaling behaviour [33]:

$$\begin{aligned} \lambda\frac{d}{d\lambda}O_1(\lambda) &= 0 \\ \lambda\frac{d}{d\lambda}O_8(\lambda) &= \frac{16}{27\pi}\alpha_s(\lambda)\,\frac{(2J+1)O_1}{m^2} \end{aligned} \tag{20}$$

With the help of (20) and (9,10) it is straightforward to show that

$$\lambda\frac{dD_{g\to\chi_{cJ}}^{(0)}}{d\lambda} = 0\ . \tag{21}$$

This is in accordance with the general expectation that physical quantities, such as fragmentation functions, are renormalization-group invariants, i.e. independent of the arbitrary factorization scale λ. (In practice, yet, it might not always be easy to know at which value of λ the matrix elements are evaluated.)

To leading order in α_s the evolution equations (20) can be solved analytically with the result

$$O_8(m) = O_8(\lambda) + \frac{16}{27\beta_0}\ \ln\frac{\alpha_s(\lambda)}{\alpha_s(m)}\,\frac{(2J+1)O_1}{m^2}\ . \tag{22}$$

This solution may be used to provide an order-of-magnitude estimate of the colout-octet matrix element O_8 in terms of the colour-singlet matrix element O_1 by assuming that $O_8(\lambda)$ can be neglected compared to the second term in (22) for $\alpha_s(\lambda) = 1$. Recall that, to leading order in v^2, $O_1 = 9|R'_P(0)|^2/2\pi$. Note also that, solving (20) for constant α_s, one recovers the approximate solution (10).

The new factorization approach provides a consistent framework for the calculation of P-wave production and decays; χ_{cJ} decays can well be described and a reasonable value of $\alpha_s(m)$ is found [19]. Detailed comparisons of χ_{cJ} production with experiments have not yet been performed. Based on (18) or (8) one expects χ_{cJ} production rates to be approximately proportional to $(2J+1)$. Preliminary CDF data [35] on the χ_{c1} to χ_{c2} ratio at high p_T, where gluon fragmentation is the dominant production mechanism, indeed seem to confirm this expectation.

The comparison is less fortunate for the total production rates measured at fixed-target energies. Experimentally, the ratio of χ_{c1} to χ_{c2} production is about $2:3$ [19]. This still seems to hold at $\sqrt{s}$ sufficiently large for the gluon fusion to dominate over quark-initiated processes. However, one then expects, theoretically, $\sigma(\chi_{c1})/\sigma(\chi_{c2}) = 0$ in leading order in v^2 and $\alpha_s(m)$: The Landau–Yan theorem forbids χ_{c1} production through the fusion of two gluons, hence the colour-singlet matrix element $\langle 0|\mathcal{O}_1^{\chi_{c1}}(8,{}^3P_1)|0\rangle$ does not contribute at $O(\alpha_s^2)$. However, there is no contribution either from the colour-octet matrix element $\langle 0|\mathcal{O}_8^{\chi_{c1}}(6,{}^3S_1)|0\rangle$: two-gluon fusion into a coloured ${}^3S_1$ state is absent, since in

the non-relativistic limit the corresponding amplitude is equal to zero. Hence corrections to the ratio are truly of $O(\alpha_s(m))$ or of $O(v^2)$, i.e. there is no $O(v^2)$ correction that is enhanced by a short-distance factor $1/\alpha_s(m)$. (Such a correction does, however, exist in the case of $q\bar{q}$ annihilation.)

Similar problems exist in the description of J/ψ (and ψ', collectively denoted by ψ in the following) production and decays. Up to and including the $O(v^2)$ its Fock-state expansion is

$$\begin{aligned} |\psi(1^{--})\rangle \;=\; & O(1)|Q\bar{Q}(^3S_1,\underline{1})\rangle + \; O(v)|Q\bar{Q}(^3P_J,\underline{8})g\rangle \\ & + \sum_{c=1,8}\Big\{O(v^2)|Q\bar{Q}(^3S_1,\underline{c})gg\rangle + O(v^2)|Q\bar{Q}(^3D_J,\underline{c})gg\rangle\Big\} \\ & + O(v^2)|Q\bar{Q}(^1S_0,\underline{8})g\rangle + O(v^3)\;. \end{aligned} \tag{23}$$

Hence corrections to the predictions of the colour-singlet model are truly of $O(v^2)$, i.e. to $O(1)$ the new factorization approach coincides with the colour-singlet model that is known to be way-off the data. Large relativistic corrections are therefore needed.

In the context of a meaningful expansion in powers of v^2, large relativistic corrections can only be accommodated if contributions, suppressed by power(s) of v^2 become important because the leading contribution is suppressed by additional power(s) of $\alpha_s(m)$. However, the $O(v^2)$ corrections are not enhanced by a short-distance factor $1/\alpha_s(m)$ since they are genuine $O(v^2)$ corrections to the production of a colour-singlet $^3S_1$ state, cf. (17). Only at $O(v^4)$ does such an enhancement occur: a factor $1/\alpha_s(m)$ in gluon–gluon fusion to J/ψ via $\langle 0|\mathcal{O}_8^\psi(6,{}^1S_0)|0\rangle$ and $\langle 0|\mathcal{O}_8^\psi(8,{}^1P_{0,2})|0\rangle$ (relevant for ψ production at fixed-target energies), and a factor $1/\alpha_s^2(m)$ in gluon fragmentation into ψ via $\langle 0|\mathcal{O}_8^\psi(6,{}^3S_1)|0\rangle$. Treating the latter matrix element as a free parameter, the description of high-p_T ψ' production at the Tevatron can indeed be rescued [34], but clearly more work is needed before the new factorization formalism is established as (the) successful theory of quarkonium production.

Further work can come from three sources. First, further phenomenological studies are needed. Ideally, one would like to have a global analysis of the data on charmonium production from all high-energy processes. Comparisons with bottomonium production should confirm that relativistic corrections indeed decrease as the heavy-quark mass increases.

Secondly, more theoretical analyses of the foundation of the factorization formalism of NRQCD [33] in (full) QCD are needed. A key ingredient is the velocity-scaling rules, both for the ordering of operators of a given dimension and the Fock-state expansion. Using perturbation theory, each additional gluon associated with the (assumed) dominant $Q\bar{Q}$ pair is ascribed an extra power of v via the identification $v \sim \alpha_s(mv)$, valid for a colour-Coulomb potential. Although this estimate may be underlined by the multipole expansion, we do not know of any rigorous derivation. One way would be the extension of the factorization of

HQ$\overline{\text{Q}}$ET [32] from quarkonium decays to their production. Additionally, implications of spin symmetry [36] for the production (and decays) of heavy quarkonia should be investigated further.

Thirdly, more experimental data will improve our understanding of bound states of heavy quarks. Concerning their production, one would in particular like to see ratios of the production rates of various charmonium states; as a function of p_T at the Tevatron and HERA, and their x_F dependence in hadro- and photoproduction. Interesting would also be the observation of a spin alignment of the heavy quarkonium states. Last but not least, valuable information will come from charmonium production in e^+e^- collisions through improved measurements of b-decays into charmonium, observation of a fragmentation contribution, and (at LEP2) charmonium production in two-photon collisions.

Acknowledgements

I am grateful to M. Mangano, G. Ridolfi, and R. Vogt for providing me with figures from their works.

References

[1] P. Nason, S. Dawson and R.K. Ellis, Nucl. Phys. **B303** (1988) 607 and **B327** (1988) 49;
W. Beenakker, R. Meng, G.A. Schuler, J. Smith and W.L. van Neerven, Nucl. Phys. **B351** (1991) 507 and Phys. Rev. **D40** (1989) 54

[2] R.K. Ellis and P. Nason, Nucl. Phys. **B312** (1989) 551;
J. Smith and W.L. van Neerven, Nucl. Phys. **B374** (1992) 36

[3] E. Laenen, S. Riemersma, J. Smith and W.L. van Neerven, Nucl. Phys. **B392** (1993) 162; ibid. 229

[4] M. Drees, M. Krämer, J. Zunft and P.M. Zerwas, Phys. Lett. **B306** (1993) 371

[5] E. Laenen, S. Riemersma, J. Smith and W.L. van Neerven, Phys. Rev. **D49** (1994) 5753

[6] S. Frixione, M.L. Mangano, P. Nason and G. Ridolfi, Nucl. Phys. **B412** (1994) 225

[7] B.W. Harris and J. Smith, Stony Brook preprint ITP-SB-94-06, January 1995 (hep-ph/9502312) and ITP-SB-95-08 in preparation

[8] S. Frixione, M.L. Mangano, P. Nason and G. Ridolfi, Nucl. Phys. **B431** (1994) 453

[9] P. Harriman, A.D. Martin, R.G. Roberts and W.J. Stirling, Phys. Rev. **D37** (1990) 798;
P.J. Sutton, A.D. Martin, R.G. Roberts and W.J. Stirling, Phys. Rev. **D45** (1992) 2349

[10] R.V. Gavai, S. Gupta, P.L. McGaughey, E. Quack, P.V. Ruuskanen, R. Vogt and X.-N. Wang, Darmstadt preprint GSI-94-76, November 1994

[11] M. Glück, E. Reya and A. Vogt, Z. Phys. **C53** (1992) 127

[12] A.D. Martin, W.J. Stirling and R.G. Roberts, Phys. Lett. **B306** (1993) 145

[13] TOPAZ collaboration, R. Enomoto et al., Phys. Lett. **B328** (1994) 535, Phys. Rev. **D50** (1994) 1879;
VENUS collaboration, S. Uehara et al., Z. Phys. **C63** (1994) 213

[14] A. Finch for the ALEPH collaboration, in Proc. of the Workshop on Two-Photon Physics at LEP and HERA, eds. G. Jarlskog and L. Jönsson, Lund, Sweden, May 1994

[15] S.J. Brodsky, P. Hoyer, A.H. Mueller and W.-K. Tang, Nucl. Phys. **B369** (1992) 519

[16] I. Abt et al. (H1), Nucl. Phys. **B407** (1993) 515;
M. Derrick et al. (Zeus), Phys. Lett. **B316** (1993) 412

[17] A.D. Martin, W.J. Stirling and R.G. Roberts, Phys. Rev. **D50** (1994) 6734

[18] M.B. Einhorn and S.D. Ellis, Phys. Rev. **D12** (1975) 2007;
H. Fritzsch, Phys. Lett. **B67** (1977) 217;
M. Glück, J.F. Owens and E. Reya, Phys. Rev. **D17** (1978) 2324;
J. Babcock, D. Sivers and S. Wolfram, Phys. Rev. **D18** (1978) 162

[19] For a recent review, see G.A. Schuler, "Quarkonium production and decays", preprint CERN-TH.7170/94, February 1994, to appear in Phys. Rep.

[20] C.H. Chang, Nucl. Phys. **B172** (1980) 425;
E.L. Berger and D. Jones, Phys. Rev. **D23** (1981) 1521;
R. Baier and R. Rückl, Phys. Lett. **B102** (1981) 364 and Z. Phys. **C19** (1983) 251;
J.G. Körner, J. Cleymans, M. Kuroda and G.J. Gounaris, Phys. Lett. **B114** (1982) 195 and Nucl. Phys. **B204** (1982) 6

[21] J.H. Kühn and H. Schneider, Phys. Rev. **D24** (1981) 2996 and Z. Phys. **C11** (1981) 263

[22] E. Braaten and T.C. Yuan, Phys. Rev. Lett. **71** (1993) 1673

[23] E. Braaten, K. Cheung and T.C. Yuan , Phys. Rev. **D48** (1993) 4230

[24] E. Braaten and T.C. Yuan, Phys. Rev. **D50** (1994) 3176

[25] Y.Q. Chen, Phys. Rev. **D48** (1993) 5181;
T.C. Yuan, Phys. Rev. **D50** (1994) 5664

[26] E. Braaten, M.A. Doncheski, S. Fleming and M.L. Mangano, Phys. Lett. **B333** (1994) 548

[27] M. Cacciari and M. Greco, Phys. Rev. Lett. **73** (1994) 1586;
D.P. Roy and K. Sridhar, Phys. Lett. **B339** (1994) 141

[28] D.P. Roy and K. Sridhar, Phys. Lett. **B345** (1995) 537

[29] M. Vänttinen, P. Hoyer, S.J. Brodsky and W.-K. Tang, preprint SLAC-PUB-6637, August 1994 (hep-ph-9410237)

[30] R. Gavai, D. Kharzeev, H. Satz, G.A. Schuler, K. Sridhar and R. Vogt, preprint CERN-TH.7526/94, December 1994 (hep-ph-9502270)

[31] G.T. Bodwin, E. Braaten, T.C. Yuan and G.P. Lepage, Phys. Rev. **D46** (1992) R3703

[32] T. Mannel and G.A. Schuler, preprints CERN-TH.7468/94, September 1994 (hep-ph/9410333), Z. Phys. C in press, and CERN-TH.7523/94, December 1994 (hep-ph/9412337), Phys. Lett. B in press

[33] G.T. Bodwin, E. Braaten and G.P. Lepage, Phys. Rev. **D51** (1995) 1125

[34] E. Braaten and S. Fleming, Northwestern Univ. preprint NUHEP-TH-94-26, November 1994 (hep-ph/9411365)

[35] V. Papadimitriou for the CDF collaboration, "Production of heavy quark states in CDF", talk presented at the XXXth. Rencontre de Moriond, Les Arcs, Savoie, France, March 1995

[36] P. Cho and M.B. Wise, Phys. Lett. **B346** (1995) 129

Figure 1: Lowest-order contributions to heavy-quark hadroproduction.

Figure 2: Cross sections for b and c production in πN collisions. For details see text (from ref. [8]).

Figure 3: Total charm production cross sections from pp and pA measurements compared to calculations. The curves are: MRS D$-'$ $m_c = 1.2$ GeV, $\mu = 2m_c$ (solid); MRS D0$'$ $m_c = 1.2$ GeV, $\mu = 2m_c$ (dashed); GRV HO $m_c = 1.3$ GeV, $\mu = m_c$ (dot-dashed); GRV HO $m_c = 1.5$ GeV, $\mu = m_c$ (dotted) (from ref. [10]).

Figure 4: The b-quark cross sections at CDF. For details see text (from ref. [8]).

Figure 5: Preliminary CDF data for prompt J/ψ and ψ' production compared with theoretical predictions of the total fragmentation contribution (solid curves) and the total leading-order contribution (dashed curves) (from ref. [26]).

Figure 6: The ratio of $(\chi_{c1} + \chi_{c2}) \to J/\psi$ to total J/ψ production as a function of c.m. energy $\sqrt{s}$, by proton (open symbols) and pion beams (solid symbols) (from ref. [30]).

Figure 7: The ratio of ψ' to J/ψ production as a function of c.m. energy $\sqrt{s}$, on proton (circles) and nuclear targets (squares) (from ref. [30]).

Figure 8: The ratio of ψ' to J/ψ production as a function of transverse momentum; the shaded strip shows the average value of Fig. 7 (from ref. [30]).

Figure 9: The differential J/ψ production cross section $(d\sigma[pN \to J/\psi X]/dy) = 2.5 \times 10^{-2}$ $(d\tilde{\sigma}[c\bar{c}]/dy)$ at $y = 0$, calculated with MRS D$-'$ PDF, compared with data (from ref. [30]).

Figure 10: Energy dependence of Υ production in pN collisions using the MRS D$-'$ PDF. Also shown (CR) is a phenomenological low-energy fit (from ref. [30]).

Figure 11: The J/ψ longitudinal momentum distributions compared with $\bar{p}N$ (top) and pN (bottom) data using two parametrizations of the PDF, MRS D$-'$ (solid) and GRV (dashed) (from ref. [30]).

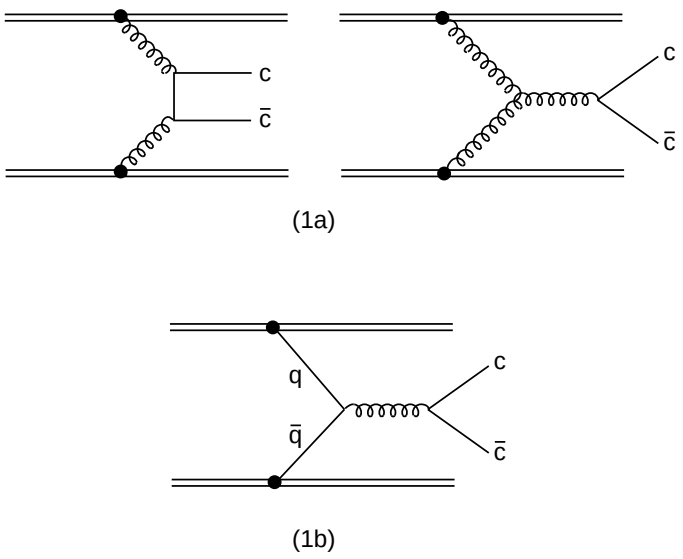

Figure 1: Lowest-order contributions to heavy-quark hadroproduction.

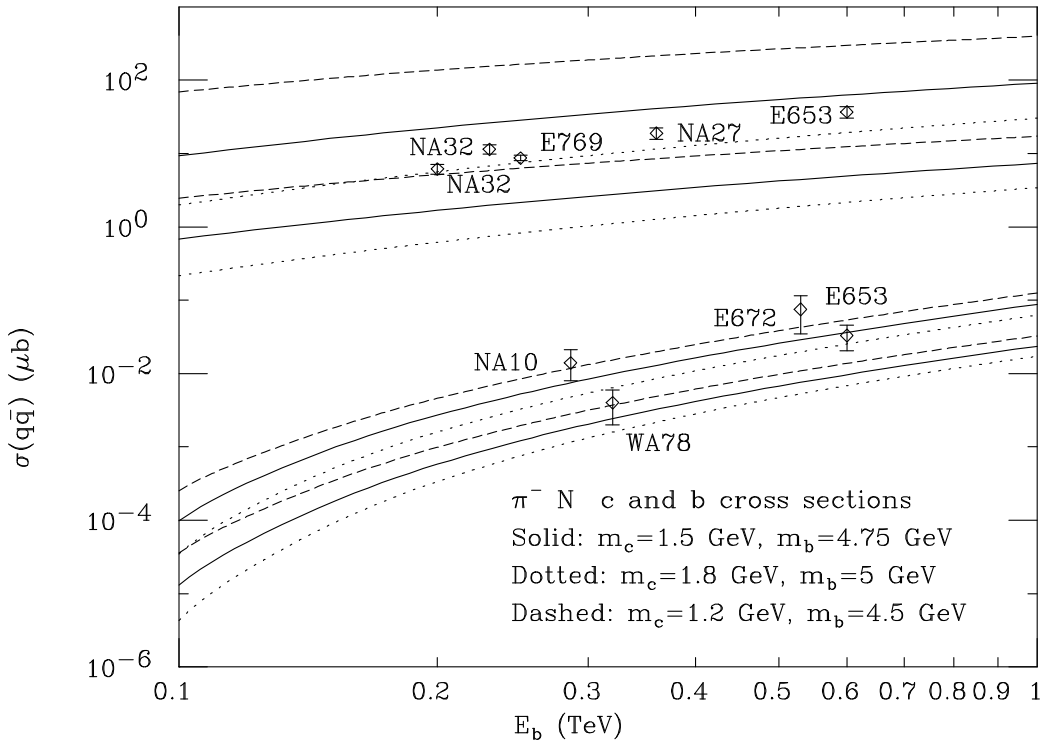

Figure 2: Cross sections for b and c production in πN collisions. For details see text (from ref. [8]).

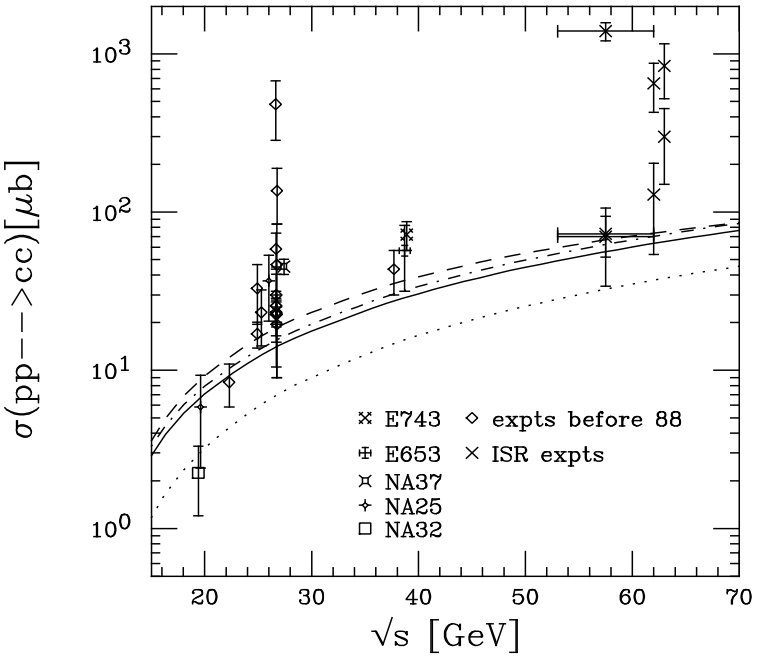

Figure 3: Total charm production cross sections from pp and pA measurements compared to calculations. The curves are: MRS D$-'$ $m_c = 1.2$ GeV, $\mu = 2m_c$ (solid); MRS D0$'$ $m_c = 1.2$ GeV, $\mu = 2m_c$ (dashed); GRV HO $m_c = 1.3$ GeV, $\mu = m_c$ (dot-dashed); GRV HO $m_c = 1.5$ GeV, $\mu = m_c$ (dotted) (from ref. [10]).

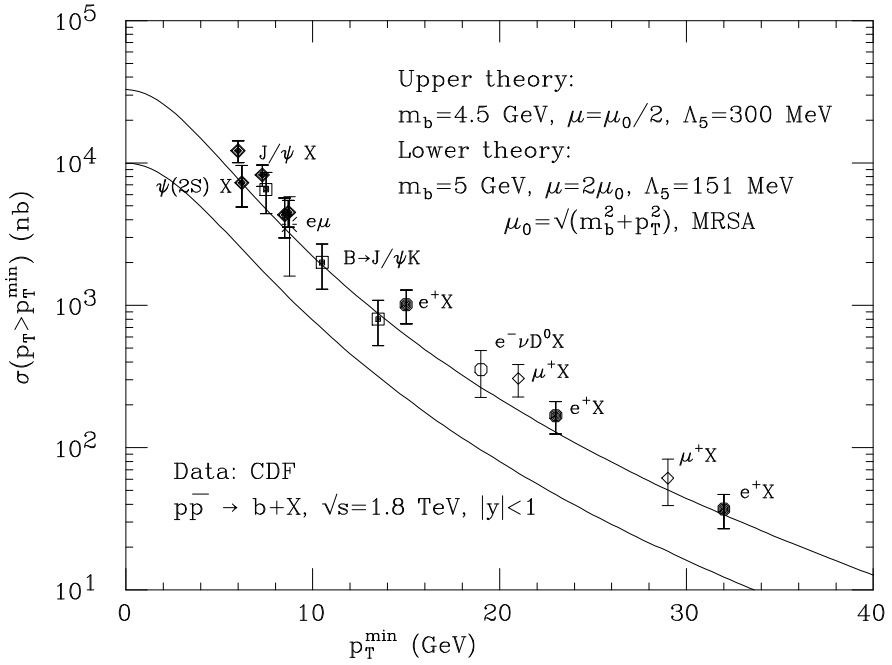

Figure 4: The b-quark cross sections at CDF. For details see text (from ref. [8]).

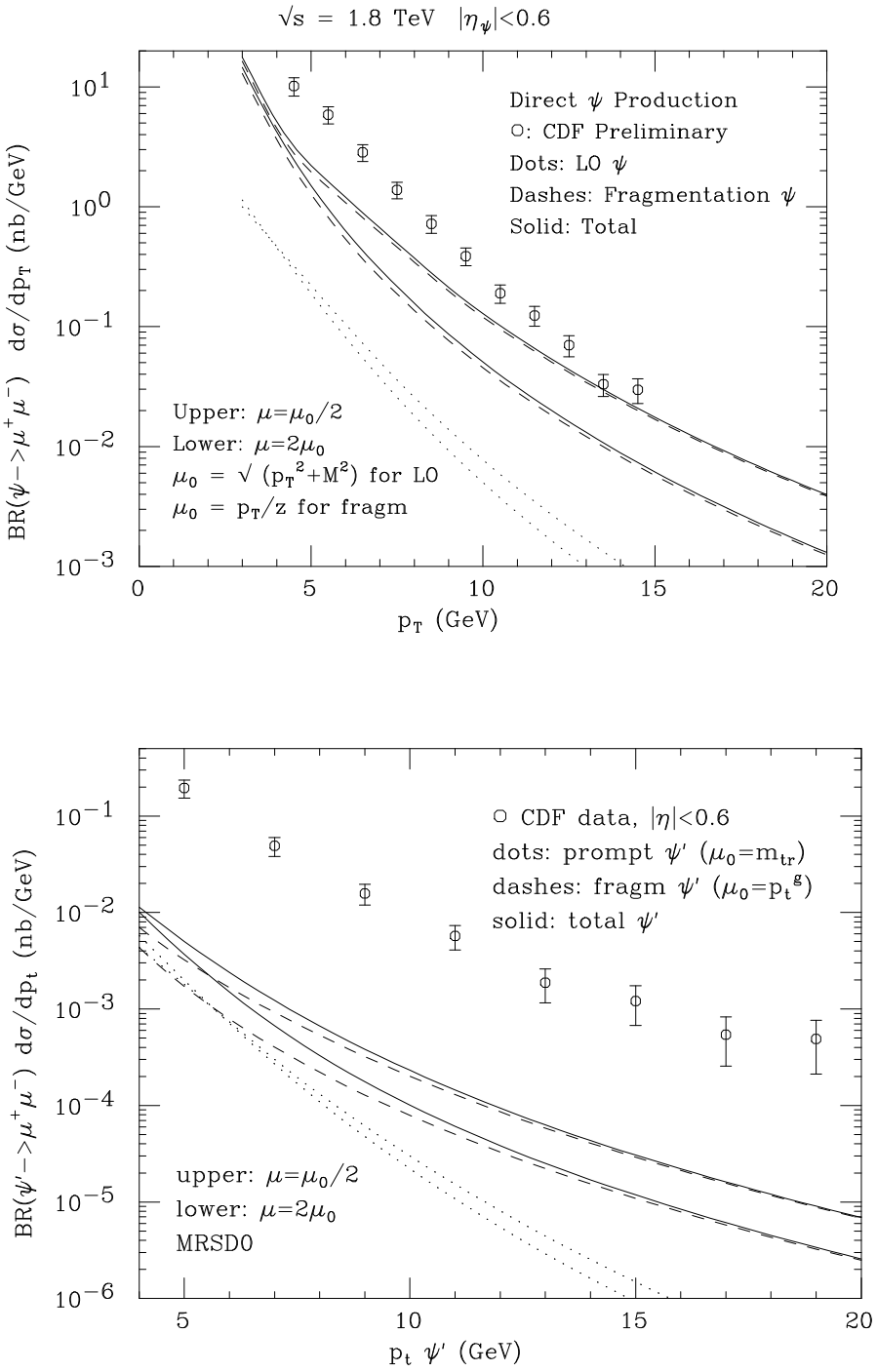

Figure 5: Preliminary CDF data for prompt J/ψ and ψ' production compared with theoretical predictions of the total fragmentation contribution (solid curves) and the total leading-order contribution (dashed curves) (from ref. [26]).

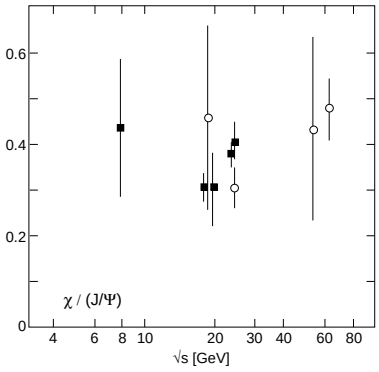

Figure 6: The ratio of $(\chi_{c1} + \chi_{c2}) \rightarrow J/\psi$ to total J/ψ production as a function of c.m. energy $\sqrt{s}$, by proton (open symbols) and pion beams (solid symbols) (from ref. [30]).

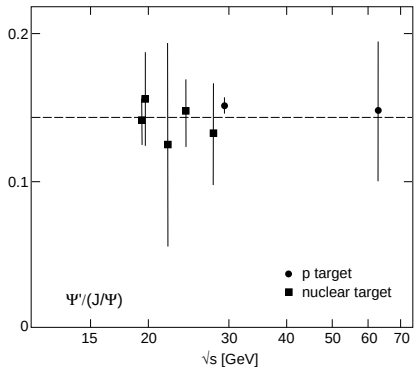

Figure 7: The ratio of ψ' to J/ψ production as a function of c.m. energy $\sqrt{s}$, on proton (circles) and nuclear targets (squares) (from ref. [30]).

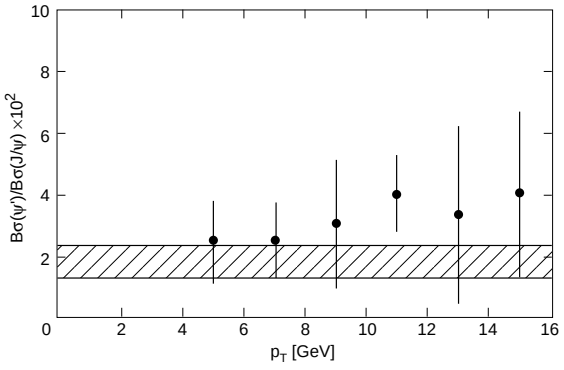

Figure 8: The ratio of ψ' to J/ψ production as a function of transverse momentum; the shaded strip shows the average value of Fig. 7 (from ref. [30]).

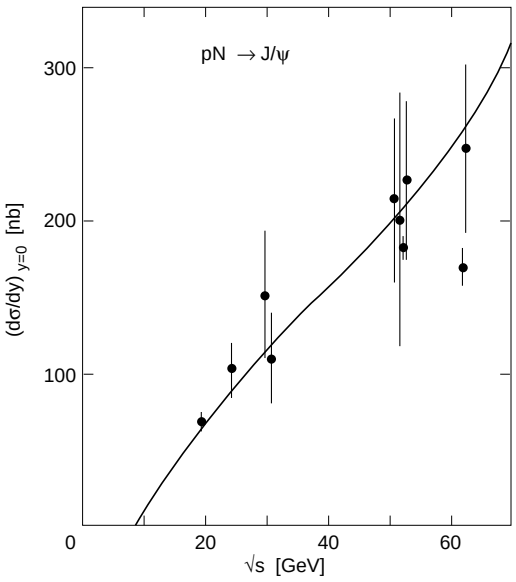

Figure 9: The differential J/ψ production cross section $(d\sigma[pN \to J/\psi X]/dy) = 2.5 \times 10^{-2}$ $(d\tilde{\sigma}[c\bar{c}]/dy)$ at $y = 0$, calculated with MRS D$-'$ PDF, compared with data (from ref. [30]).

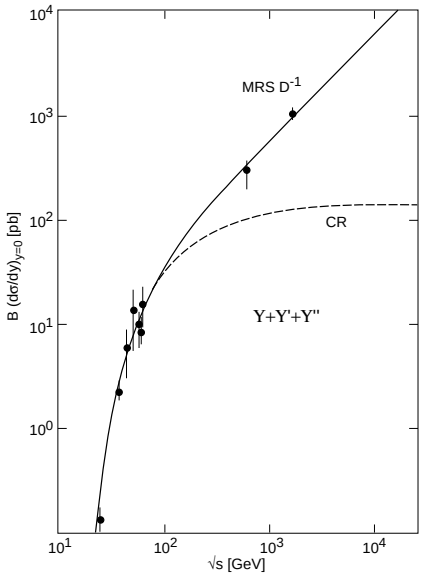

Figure 10: Energy dependence of Υ production in pN collisions using the MRS D$-'$ PDF. Also shown (CR) is a phenomenological low-energy fit (from ref. [30]).

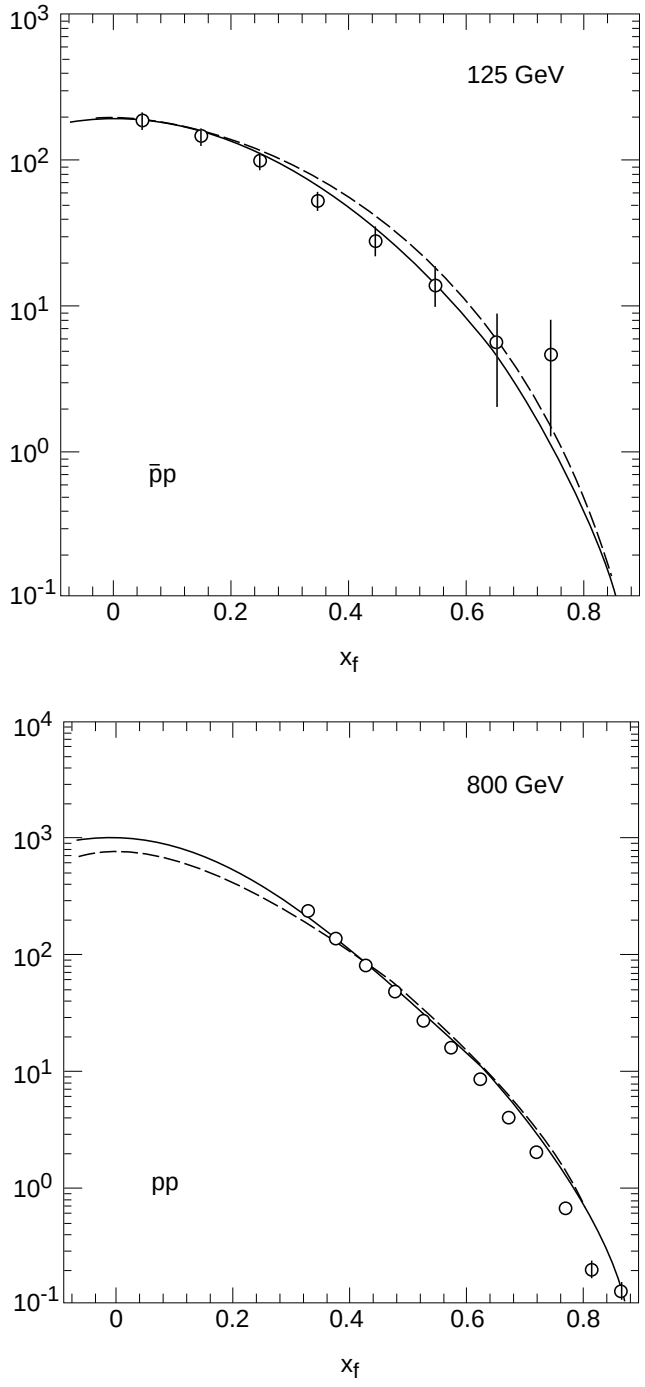

Figure 11: The J/ψ longitudinal momentum distributions compared with $\bar{p}N$ (top) and pN (bottom) data using two parametrizations of the PDF, MRS D$-'$ (solid) and GRV (dashed) (from ref. [30]).